Visual Abstract

# Identification of the anisotropic behavior of the laser welded Interstitial Free steels subjected to off-axis tensile tests

Arfaoui Latifa
*University of Tunis El Manar, ENIT, LR-MAI-ENIT, Tunisia*
*arfaoui_latifa@hotmail.fr, https://orcid.org/0000-0001-5019-7479*

Samet Amel, Znaidi Amna
*University of Tunis El Manar, IPEIEM, LR-MAI-ENIT, Tunisia*
*amel.samet@ipeiem.utm.tn, amna.znaidi@ipeiem.utm.tn*

**ABSTRACT.** The main purpose of this paper is to study the anisotropic behavior of laser welded interstitial free steel HC 260Y when it is subjected to monotonic tensile tests. The specimens were cut in different orientations according to the rolling direction, annealed and finally assembled by laser welding. The plastic behavior was modelled using an identification strategy based on a behavior law taking into account the anisotropy of this material, a hardening law describing the evolution of the hardening curves and an evolution law. The proposed identification strategy allowed for a good validation of the model. The model was afterwards used to predict the behavior of the welded material when it is subjected to various solicitations. Finally, the fracture surfaces of the specimens were examined using the scanning electron microscope (SEM) to determine the failure characteristics under the tensile loading.

**KEYWORDS.** Interstitial Free steel; Laser welding; Off-axis tensile tests; anisotropy; Identification strategy; SEM.



**Citation:** Arfaoui, L., Samet, A., Znaidi, A., Identification of the anisotropic behavior of the laser welded Interstitial Free steels subjected to off-axis tensile tests, Frattura ed Integrità Strutturale, 61 (2022) 282-293.

**Received:** 18.03.2022
**Accepted:** 29.05.2022
**Online first:** 02.06.2022
**Published:** 01.07.2022



## INTRODUCTION

With the advent of new generation automobiles, the demand of high formability steels especially Interstitial Free (IF) steels, has progressively accentuated. IF steels are mainly used in autobody fabrication. They are generally formed into intricate shapes at high production rates and manufactured by welding.
The excellent formability of IF steels is achieved through the reduction of the amount of interstitial elements, carbon and nitrogen, to an extremely low level [1-3], mainly by the addition of stabilizing elements, such as Titanium and/or Niobium [4-6].
IF steels are cold-rolled into sheets first, in order to fabricate a variety of final product components. However, the cold rolling leads to a directional microstructural texture, and thus anisotropic mechanical properties in the processed steels [7].

The Laser welding processes, of thin sheets assemblies or Tailored Welded Blanks (TWBs), have given many successful advantages in manufacturing engineering [8]. It surpasses traditional welding techniques with speed, thin welding, strength, easy integration, contactless process, and minimal maintenance costs [9].
The welded auto-components are exposed to static, impact or fatigue loading conditions because of sudden braking, vehicle crash, rough roads, etc. Numerical simulation tools are increasingly used in industry for the study of the failure of the welded joints as well as the optimization of the welding operation itself. The accuracy of all predictions made using numerical modelling strongly depends on the constitutive laws used to describe the plastic behavior of the welded material as well as the base material. For a proper mathematical modelling of its behavior at the macro-level, an accurate understanding of different effects related to the material; such as its initial anisotropy as well as its hardening is necessary.
Many studies have focused in the welding of IF steels [9,29-31]. However, there is a need to develop models that can describe the behaviour of this laser welded material under a number of loading conditions. The main objective of this paper is therefore the development, through an identification strategy followed by its validation, of a constitutive model able to describe the elastoplastic behavior of the laser welded IF steel HC260Y when it is subjected to several stresses. The anisotropic yield function proposed by Barlat was used to model the elastoplastic behavior of the welded material. The parameters of the criterion were determined based on the off-axis tensile tests performed on three loading directions (00°, 45° and 90°). The Hollomon power law was used to describe the hardening behavior of the welded steel, under the isotropic hardening assumption. The proposed model was subsequently used to predict the evolution of the Lankford coefficient depending on the off-axis angle and to determine the load surfaces for several tests. The fracture surfaces were examined by the SEM in order to characterize the fracture mechanism in the welded specimens.

## EXPERIMENTAL PLATFORM

### *Chemical composition*

In this work, cold-rolled IF steel sheets of thickness 1.2 mm have been used to prepare the tensile specimens. The chemical composition of the material is given in Tab. 1.

| C | Mn | P | Si | Ti | Al | Cr | Ni | Cu | S | Mo | Sn | B |
|---|---|---|---|---|---|---|---|---|---|---|---|---|
| 0.003 | 0.541 | 0.072 | 0.071 | 0.062 | 0.052 | 0.030 | 0.013 | 0.012 | 0.010 | 0.002 | 0.001 | 0.0004 |

Table 1: Chemical composition of the IF-Ti steel (wt %).

### *Preparation of the specimens of IF steel*

They were prepared by annealing and laser welding. They were firstly machined from the as-received parent metal by CO2 laser cutting in order to ensure that edge straightness and burr size are within the acceptable limits for laser welding. They were taken at different orientations at 0°, 45° and 90° in accordance with the rolling direction. Then, they were subjected to a recrystallization heat treatment conducted in a preheated air furnace, at 700°C for 4h 30min (Fig.1-a). The selected annealing conditions [10,13] resulted in a complete recrystallization of the specimens without development of abnormal growth of ferrite grains. The samples were laser welded in a protective Argon's atmosphere with flow rate of 0.7 bar using a 4.6 kW capacity Nd-YAG laser (Fig.1-b). The welding was made in a butt joint square groove. Run-out plates of the same material and thickness were added to ensure a uniform heat input throughout the welded section. The welding parameters are summarized in Tab. 2.

| Pulse duration (ms) | Pulse energy (J) | Laser power (KW) | Gas |
|---|---|---|---|
| 4 | 11.5 | 4 | Argon |

Table 2: Parameters of the laser welding.

In order to determine the mechanical properties of welded specimens, the tensile specimens were prepared as per ISO 4136-2013 specifications (Fig.2). The angle between the loading direction and the rolling direction will be subsequently noted ψ.

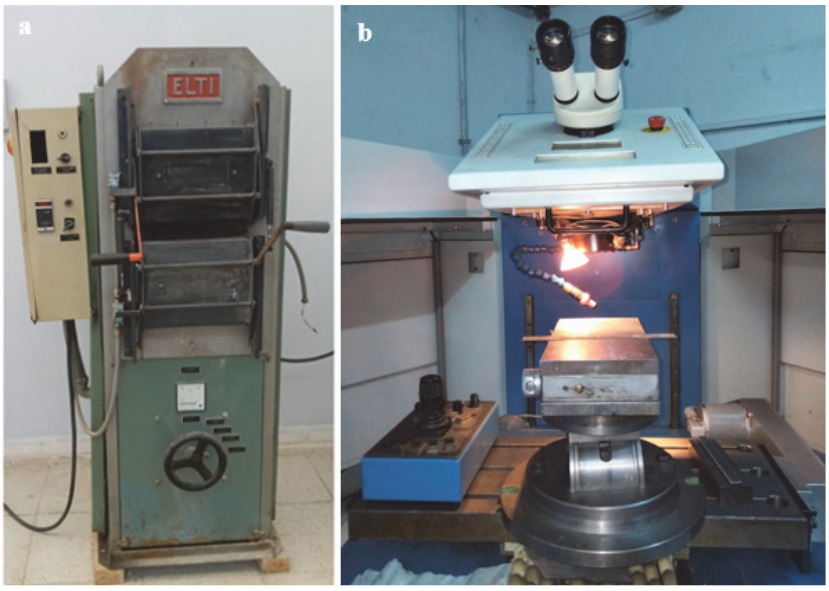


Figure 1: a) furnace and b) laser welding machine.

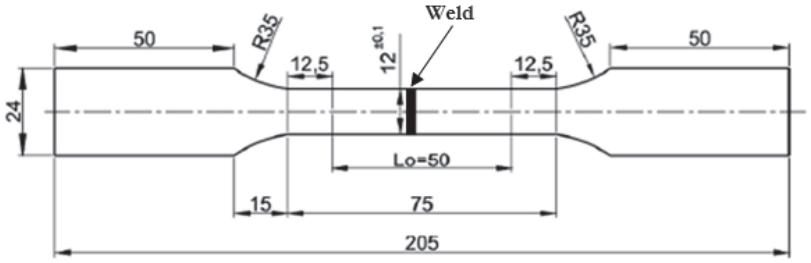


Figure 2: Specimen drawing (dimensions in mm).

*Description of the tests*

The tensile specimens were tested on a 200 kN traction compression machine (MTS Insight 200) equipped with a 0.2% precision contact extensometer (MTS 634-12F-54) (Fig. 3-a) at a constant cross-head speed of 20mm/min. The weld line was oriented at 90° with respect to the loading direction. The examinations of the fracture surfaces were conducted by means of scanning electron microscopy (SEM), using a Thermo Scientific Q250 model (see Fig. 3-b).

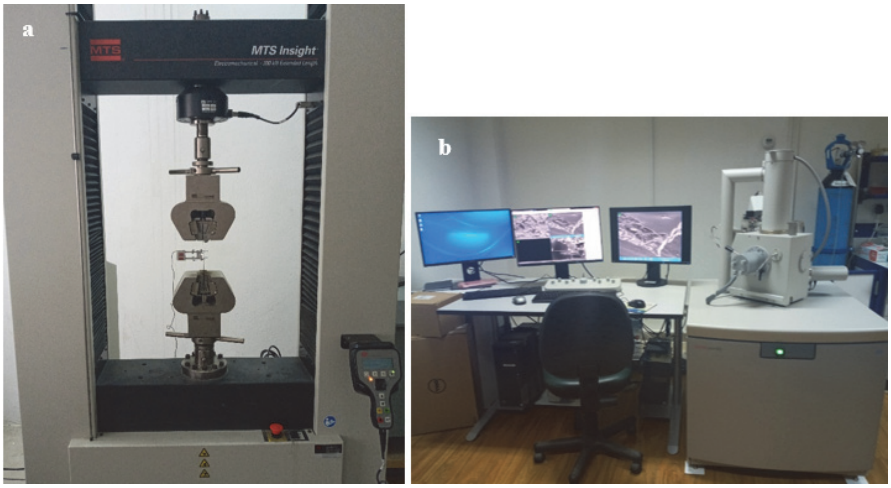


Figure 3: a) Tensile test machine and b) Scanning electron microscope.

## RESULTS AND DISCUSSION

The stress-strain curves have been plotted for different loading directions (Fig. 4). The mechanical properties of the welded material have been summarized in Tab. 3 as follows: E - Young modulus of elasticity, A% - specimen maximum elongation, $R_m$ – ultimate tensile strength, $R_e$ – yield strength (proof strength at 0.2% elongation).

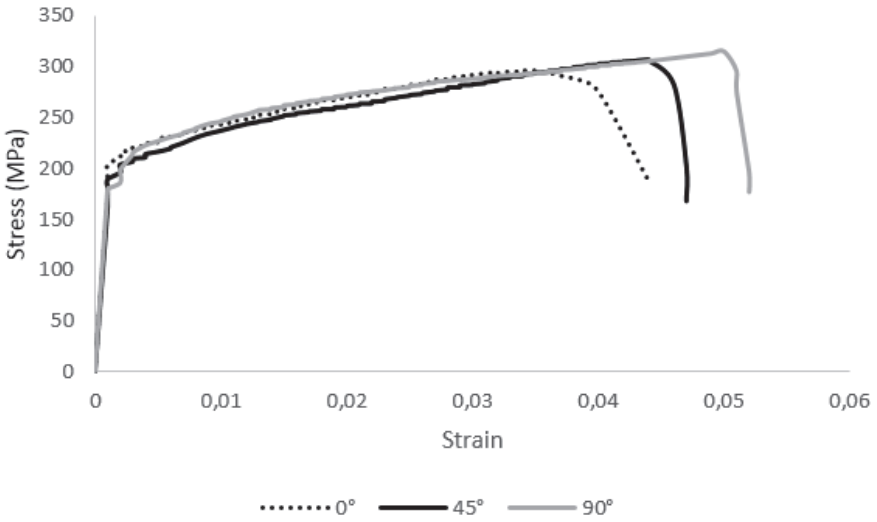


Figure 4: Stress-strain curves of the welded IF steel loaded in different orientations from the rolling direction.

| Direction | $R_e$ (MPa) | $R_m$(MPa) | E (GPa) | A% |
|---|---|---|---|---|
| 00° | 221 | 295.52 | 179.89 | 5.44 |
| 45° | 208 | 307.54 | 149.82 | 4.73 |
| 90° | 215 | 315.1 | 180.09 | 5.04 |

Table 3: Mechanical properties of the welded specimens.

The considered steel exhibits an anisotropic behavior that is shown by the variation of the mechanical properties with the in-plane direction [14-16]. However, it is noticed that the hardening curves present extremely similar mechanical properties above 0.35 % in strain.
The highest values of the maximum tensile strength and the percent of elongation were principally found in the transverse direction. In addition, the yield strength measured in this direction was less than that of the RD. Thus, the specimens cut parallel to the transverse direction exhibit the best characteristics in terms of ductility and formability.

## SEM OBSERVATIONS

The fracture morphology of the welded specimens, illustrated in Fig. 5, consists mainly in a transgranular cleavage fracture, which explains the significant decrease in the mechanical characteristics of the welded material, particularly elongation percentage [7, 20]. In fact, the microstructural examination of the heat affected zone reveals the presence of coarse grains. The rapid growth of massive ferrite caused strain in the matrix, which was relieved by the production of dislocations. As a result, grains with irregular boundaries containing numerous dislocations appeared and became a typical feature of massive ferrite. The ferrite formed was subjected to tempering during the cooling phase. Therefore, the accumulated dislocations in massive ferrite subsequently formed cell structures [24,25]. The specimen is deformed plastically. The cleavage initiates, under the combined action of the dislocations and the applied stress, from the fracture of a brittle particle (a carbide or a non- metallic inclusion) located in the grain boundary [26-28]. The material fails along well defined crystallographic planes within the grain but the crack path is affected by grain boundaries and inclusions.
The laser welding reduces the ductility and the formability of the material which leads to defects such as wrinkles, earing, and shearing in drawing, splits and wrinkles in stamping and thinning and buckling in bending.

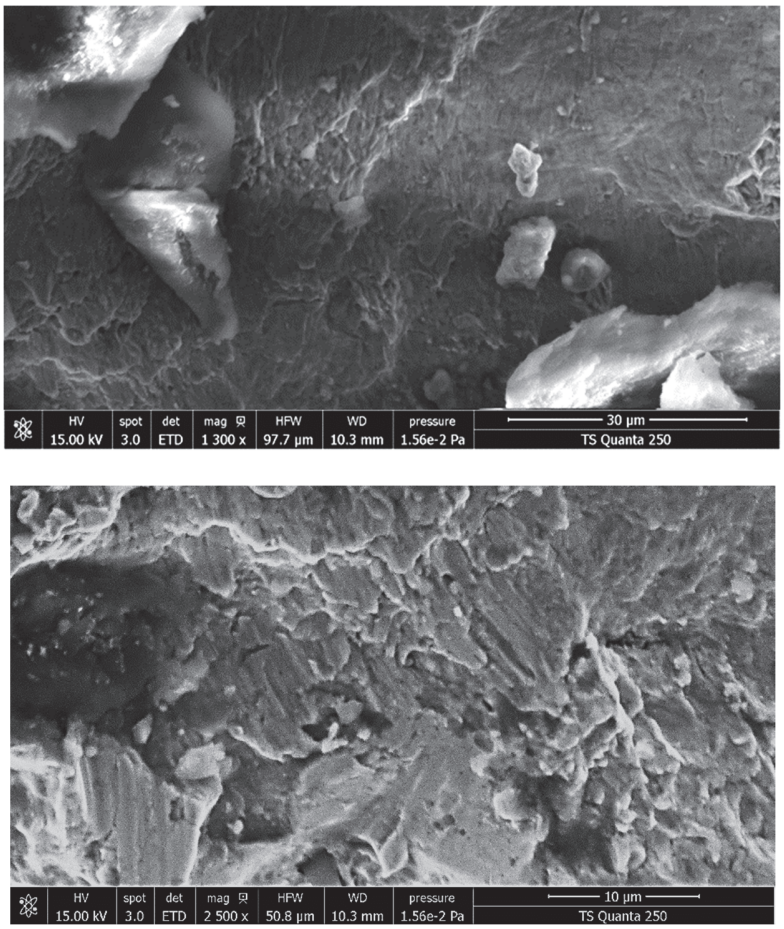


Figure 5: SEM fractgraphs.

## CONSTITUTIVE MODEL

This work is limited to the study of the plastic orthotropic behavior. The material is considered incompressible with negligible elastic deformation. The material is initially orthotropic and remains orthotropic; the isotropic hardening is represented by a single scalar hardening internal variable called $\varepsilon^P$. The behavior model is defined by:

### *Yield function*

The elastic range is considered to be evolving homothetically. The yield function can be written as follows:

$$f(q,\varepsilon^P) = \sigma_e(q) - \sigma_s(\varepsilon^P) \tag{1}$$

where f is the yield function, $\sigma_s$ is the isotropic hardening function, $\varepsilon^P$ is the equivalent plastic strain and $\sigma_e$ is the equivalent stress given by the Barlat criterion [17] as below:

$$\sigma_e(q) = (|q_I - q_{II}|^m + |q_{II} - q_{III}|^m + |q_I - q_{III}|^m)^{(\frac{1}{m})} \tag{2}$$

where m: parameter that defines the shape of the load surface; $q_I$, $q_{II}$ and $q_{III}$ are the eigenvalues of the tensor $q$ defined by the following equation:

$$q = A : \sigma^D \tag{3}$$

$A$ 4th order tensor of the linear transformation; $\sigma^D$ the deviator of the Cauchy stress tensor

*Hardening law*

Due to its simplicity, the Hollomon power law is commonly used to characterize the isotropic hardening behavior of metals and alloys [18].

$$\sigma_s(\varepsilon^P) = k_1(\varepsilon^P)^{n_1} \tag{4}$$

where $\sigma_s(\varepsilon^P)$ is the isotropic hardening function, $\varepsilon^P$ is the plastic strain, $k_1$ is the strength coefficient and $n_1$ is the strain hardening exponent. $k_1$ and $n_1$ are material parameters to be identified.

*Plastic flow law*

The associated flow rule is given by:

$$\dot{\varepsilon}^P = \dot{\lambda}\frac{\partial f}{\partial \sigma^D} \tag{5}$$

The direction of the plastic strain rate $\dot{\varepsilon}^P$ is perpendicular to the yield surface. The plastic multiplier $\dot{\lambda}$ defines its magnitude. It can be determined from the consistency condition $\dot{f} = 0$.

*Anisotropy coefficient*

The Lankford coefficient measures the variation of the plastic behavior with direction [19]. It is given by the following expression:

$$r_\psi = \frac{\dot{\varepsilon}_2}{\dot{\varepsilon}_3} \tag{6}$$

where $\dot{\varepsilon}_2$ and $\dot{\varepsilon}_3$ are the in-plane and through-the-thickness plastic strain rates, respectively. The subscript $\psi$ specifies the angle between the specimen axis and the rolling direction.

## IDENTIFICATION PROCEDURE:

The following assumptions were taken into account in order to simplify the identification process:

- The condition of incompressibility was considered (the volume remains constant during the plastic deformation).
- The plane stress assumption was adopted (thin steel sheet).
- The material behavior was considered as rigid plastic (negligible elastic deformation).
- The isotropic hardening assumption was adopted and the plasticity surface was considered to be evolving homothetically.

*Identification of the hardening curves*

The Hollomon hardening rule was curve-fitted to the stress-strain curves obtained from the uniaxial tensile tests (Fig. 6). The minimization of the quadratic error between the theoretical and experimental results allowed the identification of the hardening parameters corresponding to the mentioned law. Comparing the hardening exponent values, identified for different tests, it can be noticed that the

exponent $n_1$ is independent of the loading direction (Tab. 4). By convention, the value corresponding to the rolling direction, $n_1 = 0.143$, is considered as reference [20-23]. The hardening coefficients $k_1$, calculated for this value of $n_1$ considering the Hollomon law, are summarised in Tab. 5.

| ψ | 00° | 45° | 90° |
|---|---|---|---|
| $k_1$ | 464.9342 | 466.1388 | 471.5584 |
| $n_1$ | 0.1430 | 0.14785 | 0.1403 |

Table 4: Identification of the Hollomon law parameters for the welded specimens.

| ψ | 00° | 45° | 90° |
|---|---|---|---|
| $k_1$ | 464.9342 | 457.1954 | 422.3050 |

Table 5: Identification of the parameter $k_1$ for the fixed value of $n_1$ =0.143.

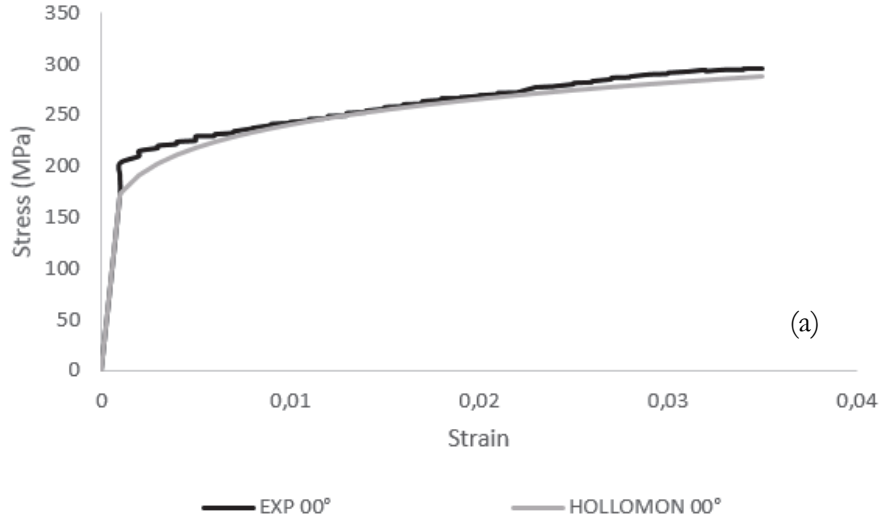


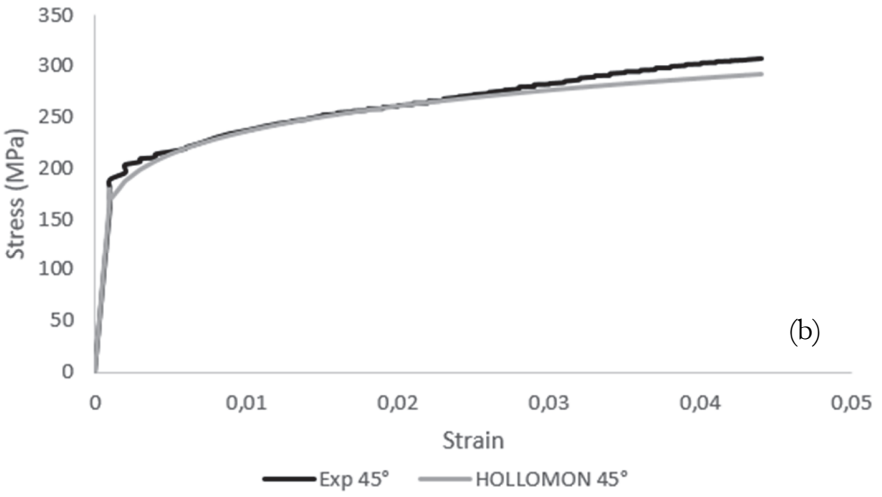

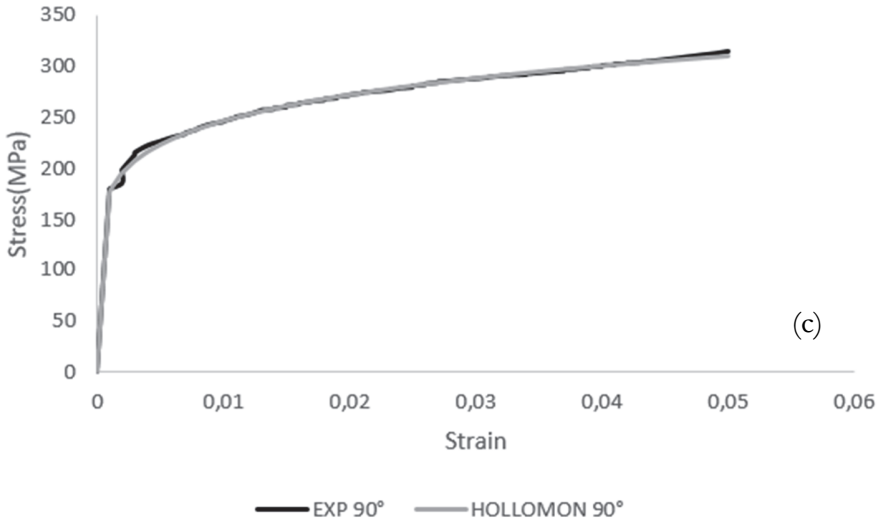


Figure 6: Identification of the hardening curve for (a) $\psi$ = 00°, (b) $\psi$ = 45° and (c) $\psi$ = 90°.

*Identification of the shape coefficient m and the anisotropy coefficients based on the hardening curves:*

The parameters of the Barlat criterion [20], in terms of anisotropy coefficients and shape coefficient, were identified through the minimization of an objective function (Eqn. 7) representing the square deviation between the theoretical and the experimental values of the parameter $k_1$, denoted $k_1(th)$ and $k_1(exp)$ respectively (Tab. 6). The optimisation algorithm was developed under Matlab. In the case of plane stresses, the number of plastic anisotropy parameters is reduced to four (f, g, h and n).

$$E = \sum_i (k_1(exp) - k_1(th))^2 \tag{7}$$

| Parameters | f | g | h | n | m |
|---|---|---|---|---|---|
| Values | 0.2399 | 0.3947 | 0.3279 | 1.2425 | 5.7876 |

Table 6: identification of the anisotropic coefficients and the shape coefficient m.

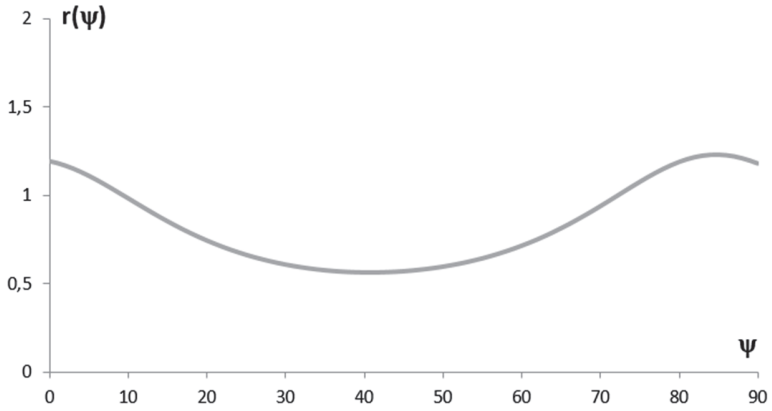


Figure 7: Evolution of the Lankford coefficient depending on the off-axis angle .

Based on the identified parameters, the evolution of the Lankford coefficient according to the off-axis angle $\psi$ was represented in Fig. 7. The minimum Lankford coefficient value was measured at $\psi$ =45°. The highest values were related to the rolling and the transverse directions.

The estimated Lankford coefficients values as well as well as the normal anisotropy $r_n$ and the planar anisotropy $\Delta r$ ratios are presented in Tab. 7. The normal anisotropy ratio $r_n$ is lower than unity. This indicates that thinning is the preferential metal flow direction which increases the risk of failure in drawing operations.

| $r_{00}$ | $r_{45}$ | $r_{90}$ | $r_n$ | $\Delta r$ |
|---|---|---|---|---|
| 1.19 | 0.57 | 1.18 | 0.87 | 0.3 |

Table 7: Estimated Lankford coefficients values for different loading directions.

*Validation:*

In order to validate the identification strategy, the experimental tensile curve in the transverse direction and the identified anisotropic parameters of the behavior model are used. The Fig. 8 shows a good agreement between the theoretical and the experimental curves.

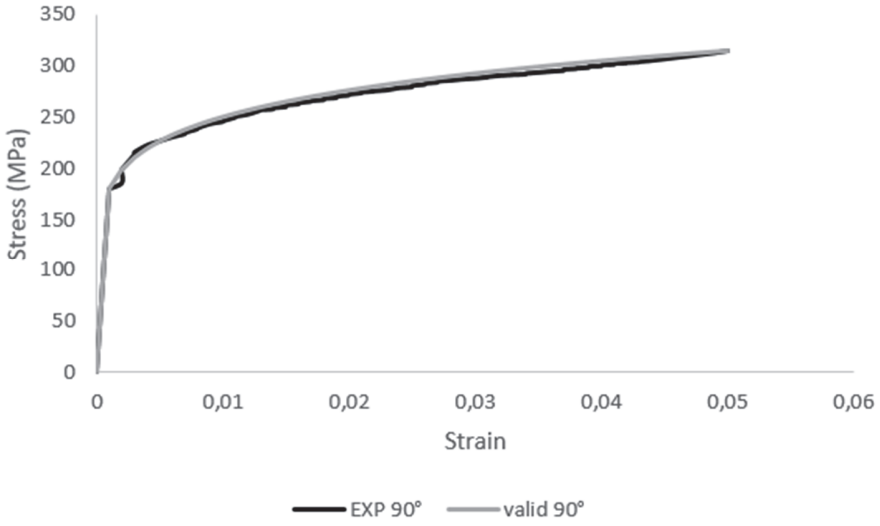


Figure 8: Validation of the hardening tensile curve for $\psi$ =90°.

## EVOLUTION OF THE YIELD SURFACE IN THE DEVIATORY PLANE $\left(\bar{x}_2, \bar{x}_3\right)$

The mechanical behavior of this material subjected to a simple tensile test, a simple shear test and planar tension test is shown in Fig. 9, through the load surfaces determined based on the proposed model in the deviatory plane $\left(\bar{x}_2, \bar{x}_3\right)$ :

$$\bar{x}_2 = |\sigma^D| \sin\theta \cos 2\psi \tag{8}$$

$$\bar{x}_3 = |\sigma^D| \sin\theta \sin 2\psi \tag{9}$$

where $\sigma^D$ is the deviator of the Cauchy stress tensor, $\psi$ is the off-axis angle and $\theta$ is the angle defining the type of the test.

The welded specimens are resistant to simple shear much better than simple tension and planar tension.

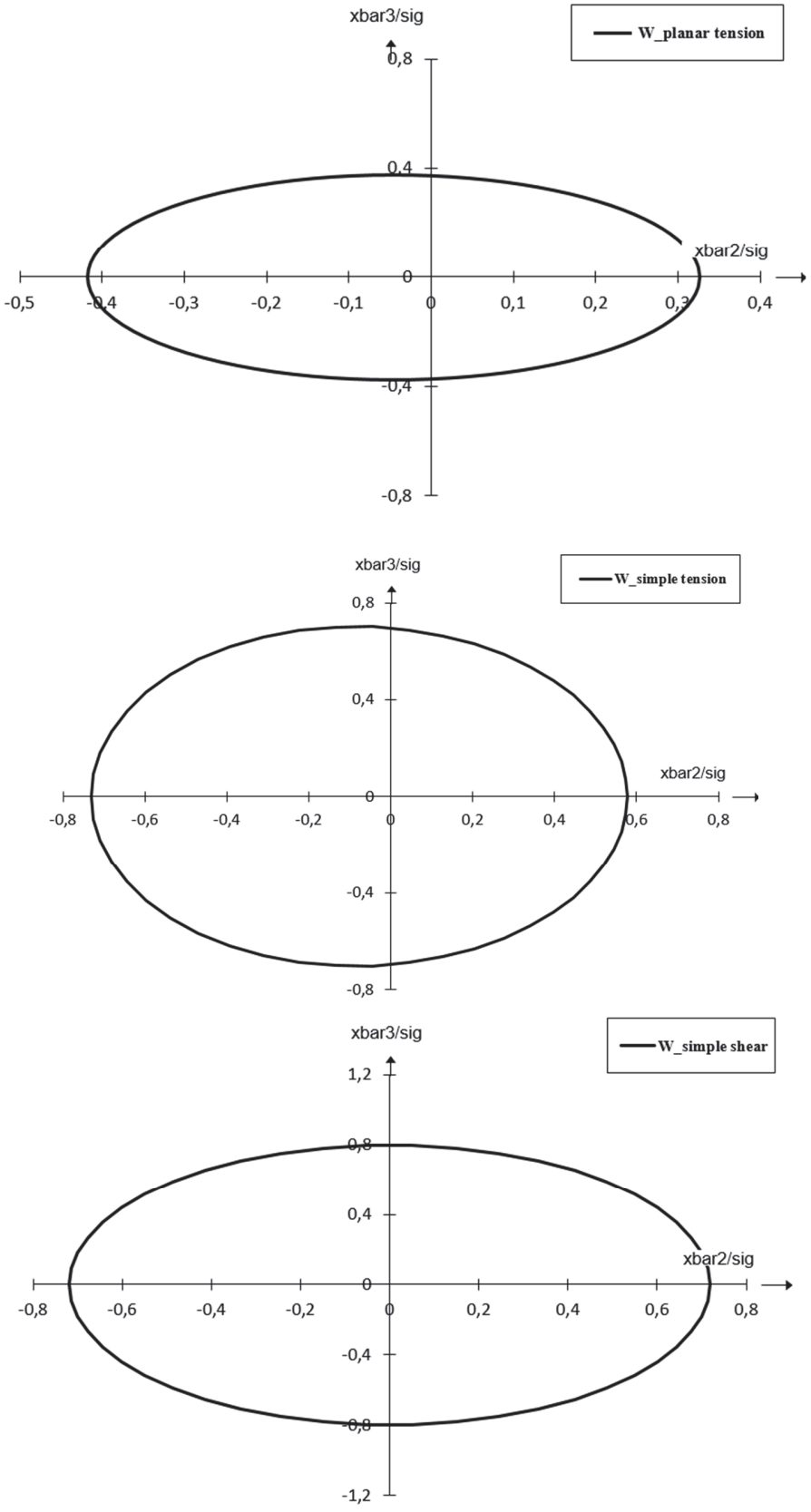


Figure 9: Evolution of the yield surface in the deviatory plane $\left(\overline{x}_2, \overline{x}_3\right)$.

## Conclusion

The model presented in this manuscript focused on the plane orthotropy in the specific case of the isotropic hardening assumption. The analytical law of Hollomon was used to describe the hardening behavior of the welded material and the yield criterion proposed by Barlat was adopted to model its elastoplastic behavior. The proposed identification methodology, based on the hardening curves obtained from the off-axis tensile tests, allowed a good validation of the model. The constitutive model was subsequently used to predict the Lankford coefficient evolution depending on the off-axis angle and to present the load surfaces relating to different mechanical tests.

The highest values of Rm and A% are related to the transverse direction. The maximum values for the Lankford coefficient correspond to the rolling direction as well as the transverse direction. The specimens cut parallel to the transverse direction exhibit the best characteristics in terms of ductility and formability.

The proposed methodology gave satisfactory results for the identification of the hardening curves and the Lankford coefficients. However, it is less satisfying for the description of the evolution of the load surfaces. In fact, improvements of the model can be considered. It would be interesting to modify the assumption of isotropic hardening used to describe the plastic behavior. Hardening variables should be further investigated by performing cyclic tests or by adopting methodologies allowing their estimation from the monotonic properties.

The examination of the fractographs corresponding to the welded specimens show a transgranular cleavage fracture. The laser welding has reduced the ductility of the material as well as its formability.

## References

[1] Tsunoyama, K. (1998). Metallurgy of ultra-low-C interstitial-free sheet steel for automobile applications, Phys Status Solidi A, 167, pp. 427–433.

[2] Chen, QZ and Duggan, BJ. (2004). On cells and microbands formed in an interstitial-free steel during cold rolling at low to medium reductions, Metall Mater Trans A Phys Metall Mater Sci, 35, pp. 3423–3430. DOI: 10.1007/s11661-004-0178-5.

[3] Arfaoui, L., Samet, A., Znaidi, A. (2022). Residual Stress Induced by Laser Welding of Interstitial Free (IF) Steel: Simulation Approach, In: Bouraoui T. et al. (eds) Advances in Mechanical Engineering and Mechanics II. CoTuMe 2021. Lecture Notes in Mechanical Engineering. Springer, Cham. DOI: 10.1007/978-3-030-86446-0_31

[4] Hoile, S. (2000). Processing and properties of mild interstitial free steels, J Mater Sci Technol ,16, pp. 1079-1093. DOI: 10.1179/026708300101506902.

[5] Khatirkar, RK., Kumar, S. (2011). Comparison of recrystallization textures in interstitial free and interstitial free high strength steels, Mater. Chem. Phys, 127(1-2), pp. 128-136. DOI: 10.1016/j.matchemphys.2011.01.045

[6] Sinha, M., Syed, B., Karmakar, A., et al. (2020). Diffusional and displacive transformations in interstitial-free steel within the scope of a critical assessment of the mechanical property, Mater. Sci. Eng. A, 787, 139519. DOI: 10.1016/j.msea.2020.139519.

[7] Arfaoui, L., Samet, A., Znaidi, A. (2020). Ductile Fracture Characterization of an IF Steel Tensile Test by Numerical Simulation, In: Aifaoui N. et al. (eds) Design and Modeling of Mechanical Systems - IV. CMSM 2019. Lecture Notes in Mechanical Engineering. Springer, Cham, pp 318-327. DOI: 10.1007/978-3-030-27146-6_34.

[8] Bayraktar, E., Kaplan, D., Yilbas, B. (2008). Comparative study: Mechanical and metallurgical aspects of tailored welded blanks (TWBs), J Mater Process Technol, 204, pp. 440-450. DOI: 10.1016/j.jmatprotec.2007.11.088.

[9] Mihaliková, M., Zgodavová, K., Bober, P. et al. (2021). The Performance of CR180IF and DP600 Laser Welded Steel Sheets under Different Strain Rates, Materials (Basel), 14(6),1553. DOI: 10.3390/ma14061553.

[10] Samet-Meziou, A., Etter, AL., Baudin, T., et al. (2008). Relation between the deformation sub-structure after rolling or tension and the recrystallization mechanisms of an IF steel, Mater Sci Eng A Struct Mater, 473(1), pp. 342-354. DOI: 10.1016/j.msea.2007.03.090.

[11] Huang, CJ. and Browne, DJ. (2006). Phase-field model prediction of nucleation and coarsening during austenite/ferrite transformation in steel,. Metall Mater Trans A Phys Metall Mater Sci, 37, pp. 589–598. DOI: 10.1007/s11661-006-0031-0.

[12] Bayraktar, E., Kaplan, D., Devillers, L., et al. (2007) Grain growth mechanism during the welding of interstitial free (IF) steels, J Mater Process Technol, 189, pp. 114–125.

[13] Bayraktar, E., Kaplan, D., Devillers, L. (2009). Physical understanding of ferrite grain growth during welding in interstitial free steels (IFS), Arab J Sci Eng, 34, pp. 115-127.
[14] Daghfas, O., Znaidi, A., Ben Ahmed, M., et al. (2017). Experimental Study on Mechanical Properties of Aluminum Alloys under Uniaxial Tensile Tests, Int J Technol, 8(4), pp. 662-672. DOI: 10.14716/ijtech.v8i4.9489.
[15] Lv, Z., Qian, L., Liu, S. et al. (2020). Preparation and Mechanical Behavior of Ultra-High Strength Low-Carbon Steel, Materials, 13(2), pp. 1-14. DOI: 10.3390/ma13020459.
[16] Sener, B., Esener, E., Firat, M. (2021). Modeling plastic anisotropy evolution of AISI 304 steel sheets by a polynomial yield function, SN Appl Sci, 3, pp. 1-12. DOI: 10.1007/s42452-021-04206-2.
[17] Barlat, F. and Brem, DLJ. (1991). A six components yield function for anisotropic materials, Int J Plast, 7, pp. 693-712
[18] Cheng, YT., Cheng, CM. (2004). Materials Science and Engineering: R: Reports, 44(4), 91.
[19] Lankford, WT., Snyder, SC., Bausher, JA. (1950). New criteria for predicting the press performance of deep drawingsheets, Trans Am Soc Met, 42, pp. 1197–1205.
[20] Arfaoui L, Samet A, Znaidi A. Characterisation of the plane anisotropy and its effect on interstitial free steel thin sheet metal forming simulation. Proceedings of the Institution of Mechanical Engineers, Part L: Journal of Materials: Design and Applications. 2022;236(3):597-610. doi:10.1177/14644207211053486.
[21] Ben Mohamed, A., Znaidi, A., Daghfas, O. et al. (2016). Evolution of Mechanical Behavior of Aluminum Alloy Al 7075 during Maturation Time, Int J Technol ,7(6). 1077. DOI: 10.14716/ijtech.v7i6.3563.
[22] Daghfas, O., Znaidi, A., Ben Mohamed, A., et al. (2017). Experimental and numerical study on mechanical properties of aluminum alloy under uniaxial tensile test, Frat ed Integrita Strutt, 11(39), pp. 263-273. DOI: 10.3221/IGF-ESIS.39.24.
[23] Harbaoui, R., Daghfas, O., Znaidi, A. (2020). Strategy for identification of HCP structure materials: study of Ti–6Al–4V under tensile and compressive load conditions, Arch Appl Mech, 90(3), pp. 1685–1703. DOI: 10.1007/s00419-020-01690-7.
[24] Liu, B., Yang, J., Wu, Y., Shen, P., Fu, J., Chen, C., Wang, S., Tsai, M., Huang, C. (2019). Investigation of massive ferrite in an interstitial-free steel, Mater. Charact, 157, pp. 153–158.
[25] Liu, BPH., Chung, TF., Yang, JR., et al. (2020). Microstructure Characterization of Massive Ferrite in Laser-Weldments of Interstitial-Free Steels, Metals, 10(7), pp. 898. DOI:10.3390/met10070898.
[26] McMahon, C. and Cohen, M. (1965). Initiation of cleavage in polycrystalline iron, Acta Metall, 13, pp. 591–604.
[27] Wallin, K. ed., (2007). Statistical Methods, In: Comprehensive Structural Integrity, Pergamon, Elsevier Science, pp. 137-157. DOI: 10.1016/B978-008043749-1/00328-0.
[28] Bousquet, A. (2013). Critère de propagation et d'arrêt de fissure de clivage dans un acier de cuve REP. Available at: https://tel.archives-ouvertes.fr/tel-00927524/document.
[29] Bayraktar, E., Kaplan, D., Buirette, C., et al. (2004). Application of impact tensile testing to welded thin sheets, J Mater Process Technol, 145, pp. 27-39. DOI: 10.1016/S0924-0136(03)00859-8.
[30] Mihaliková, M., Lišková, A., Hagarová, M., et al. (2016). Fatigue characteristics of Laser Welded DC06EK and DP600MC Steel Sheet. Conference on Micro and Nano Analysis, Gniew, Poland, 11-14 September.
[31] Dias, JS., Chuva, TC., Fonseca, MPC. (2016). Evaluation of Residual Stresses and Mechanical Properties of IF Steel Welded Joints by Laser and Plasma Processes, Mater Res, 19(3), pp. 721-727. DOI:10.1590/1980-5373-MR-2015-0558.